J. Construct. Steel Research 35 (1995) 165–187
Elsevier Science Limited
Printed in Malta.
0143-974X/95/$9.50

ELSEVIER

0143-974X(94)00034-4

Design of Steel Frames with Slender Joint-panels

Ioannis Vayas & John Ermopoulos

National Technical University of Athens, Laboratory of Steel Structures,
Patission 42, Gr-10682 Athens, Greece

&

Hartmut Pasternak

Technische Universitat Cottbus, Lehrstuhl für Stahlbau, Germany

(Received 7 March 1994; revised version received 29 June 1994; accepted 10 August 1994)

ABSTRACT

The behaviour of thin-walled slender joint-panels in knee joints of steel frames and its influence on the overall behaviour of moment-resisting frames is studied. The joint resistance is supplied by three different mechanisms. The first mechanism is the shear buckling strength of the joint-panel, which is dependent on its slenderness. The second mechanism is the tension field strength that is dependent on the relation between the dimensions of the joint-panel and its surrounding flanges. The last mechanism is the resistance due to the frame action of the joint-panel's surrounding frame. Design formulae for the evaluation of the joint resistance are derived. Monotonic and hysteretic rules for the description of the joint characteristics are proposed. Frame analyses considering the joint deformability are performed. The analytical results are compared to experimental results of joints subjected to cyclic loading.

NOTATION

The following symbols are used in this paper:

a, b	Dimensions of joint-panel
d	$\sqrt{a^2+b^2}$ Diagonal length of joint-panel
E	Modulus of elasticity
f_{yw}	Yield strength of joint-panel

f_{yr}	Yield strength of beam flanges
f_{yc}	Yield strength of column flanges
g	Width of the tension field
I_b, I_c	Moments of inertia of beam and column
l_b, l_c	Axis lengths of beam and column
M_{pr}, M_{pc}	Plastic moments of beam and column flanges
M_u, M_y	Ultimate and yield moments of joint
M_{TF}	Joint moment due to tension field action
M_{FR}	Joint moment due to the action of flanges surrounding the joint-panel
S_o, S_n	Spring forces at beginning and end of loading step
t_w	Thickness of joint-panel
t_r	Thickness of beam flanges
t_c	Thickness of column flanges
∂	Angle of inclination of the diagonal
$\bar{\lambda}=\sqrt{\frac{f_{yw}/\sqrt{3}}{\tau_{cr}}}$	Relative slenderness of joint-panel for shear buckling
σ_{bb}	Tension field stress
τ_{bb}	Shear buckling strength of joint-panel
τ_{cr}	$k_\tau \cdot 18980\ (t_w/b)^2$ in (Nmm^{-2}). Critical buckling stress of joint-panel
ϕ_u, ϕ_y	Ultimate and yield rotations of joint

1 INTRODUCTION

The performance of moment-resisting steel frames is highly influenced by the behaviour of their joints. The distribution of internal forces and moments in frames with flexible (i.e. semi-rigid) joints is different than in frames with rigid joints. In semi-rigid jointed frames a redistribution of moments from the joints to the span regions takes place. As a result, the stress conditions in the beams become more uniform and for non-sway frames a more economical design may be achieved. The flexibility of the joints also affects the overall stability of a sway frame, since it reduces its sway stiffness and results in higher interstorey drifts when the frame is subjected to horizontal loading. In the case of earthquake loading, properly designed flexible joints are able to contribute to the absorbtion of input earthquake energy, or to ductility, thus relaxing the relevant requirements for beams.

Due to its significance, a lot of experimental and theoretical research has been devoted to the study of the joint behaviour that includes both the beam-to-column connections and the joint-panel. Relevant information has recently been collected by Chen[1] and Bjorhovde *et al.*[2]

In knee joints, or in internal joints, of frames subjected to horizontal force, high shears are developed in beam-to-column joint-panels. It has been shown that these panels may contribute significantly to the ductility of the frame. Relevant design procedures are proposed by Kato *et al.*[3] All investigations are, however, limited to compact joint-panels, where yielding preceeds shear buckling.

Cases of joints with slender panels appear very often in low-rise industrial buildings, when welded plate girders are used as elements of the frames. Due to the overall geometric and loading conditions, these girders usually have compact flanges, that provide the bending resistance, and slender webs that resist the applied shear.

Slender webs exhibit a considerable post-buckling shear resistance, due to the formation of tension fields. Based on extensive research on the subject, modern codes adopt procedures that allow for the design of plate girders with slender webs in the post-critical range. These rules apply, however, only to the span region of the girders between supports.

In the belief that similar tension fields will develop in the joint region too, thus considerably increasing the carrying capacity of the joint, an extensive research programme on knee joints with thin webs has been performed. It included several tests on joints under monotonic and cyclic loading. Preliminary results for monotonic loading were presented by Scheer *et al.*[4] An evaluation of the experimental results for cyclic loading is made by Vayas *et al.*[5]

The objective of the present paper is to provide models for the description of the joint behaviour, with respect to its flexibility and strength, which are based on the experimental evidence, and to present a procedure for the evaluation of the influence of the joint behaviour on the load-carrying capacity and ductility of the frame. Both cases of monotonic and cyclic loading are treated. The design method proposed here is limited to welded joints that were examined experimentally. In the case of bolted beam-to-column connections, the influence of the connection flexibility and strength, and possibly its interaction with the relevant joint-panel characteristics, should additionally be taken into account.

2 BEHAVIOUR OF KNEE JOINTS

When a steel frame is subjected to loading, high shear stresses are developed in the joint-panels of its knee joints. The forces and moments acting around a knee joint are shown in Fig. 1. For further numerical treatment it seems advantageous to refer the joint moments and rotation to the internal corner I (Fig. 1), since the joint rotates around this corner during loading.

The experimental investigations as reported by Scheer *et al.*[6] and Vayas *et al.*[5] showed that three mechanisms contribute to the stiffness and strength of the joint. They are the ability of the joint-panel to directly resist shear stresses, the tension fields that are developed after buckling, and the frame action of the elements surrounding the joint-panel. An evaluation of the contribution of each mechanism to the joint behaviour for both positive ('closing' of the joint) and negative ('opening' of the joint) moments will be discussed subsequently.

3 JOINT RESISTANCE FOR POSITIVE MOMENTS

The shear buckling resistance of a slender joint-panel may be determined from a shear buckling curve. Adopting the relevant curve of Eurocode 3 for the webs of plate girders,[7] the ultimate shear stress is given by

$$\tau_{bb} = f_{yw}/\sqrt{3} \quad \text{for } \bar{\lambda} \leq 0{\cdot}8 \tag{1a}$$

$$\tau_{bb} = [1 - 0{\cdot}8(\bar{\lambda} - 0{\cdot}8)] f_{yw}/\sqrt{3} \quad \text{for } 0{\cdot}8 < \bar{\lambda} < 1{\cdot}25 \tag{1b}$$

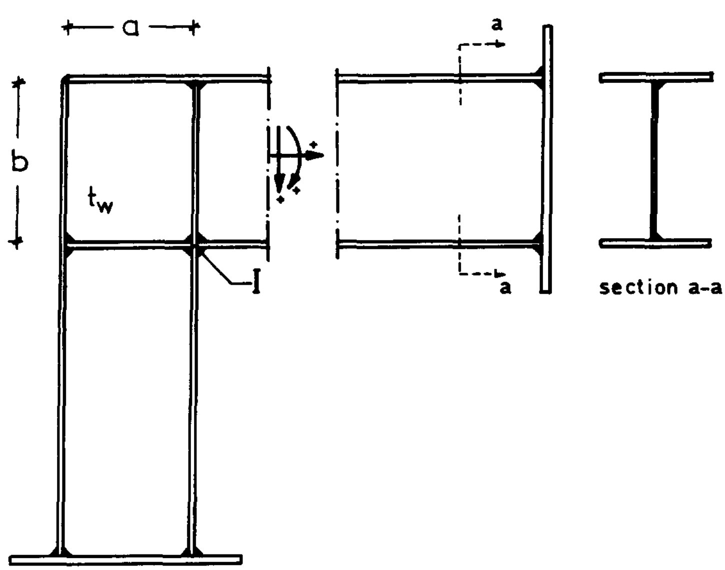

Fig. 1. Geometry of joint and sign convention for internal forces and moments.

$$\tau_{bb}=\frac{1}{\bar{\lambda}^2}\frac{f_{yw}}{\sqrt{3}}=\tau_{cr} \quad \text{for } \bar{\lambda}\geqslant 1{\cdot}25 \tag{1c}$$

where τ_{bb} is the shear buckling strength of the joint-panel; f_{yw} is its yield strength; and $\bar{\lambda}$ is the corresponding slenderness.

The relative panel slenderness, $\bar{\lambda}$, is determined from the critical, elastic shear buckling stress under the assumption that the joint-panel is simply-supported along its edges. The joint moment due to the shear buckling resistance of the joint panel is accordingly equal to

$$M_{bb}=\tau_{bb}\cdot a\cdot b\cdot t_w \tag{2}$$

where a and b are the dimensions of the joint-panel and t_w is its thickness.

Slender joint-panels exhibit a considerable post-buckling strength. This is assigned hereafter, not to the shear buckling strength, but to the tension fields that are developed after buckling, as shown in Fig. 2(a).

The anchorage of the tension field within the inner triangle (IJL) is provided by the web plates of the neighbouring beam and column sections. Outside this triangle it is provided by the flanges, so that its extension beyond it is dependent on the flange strength. When the tension field has fully developed, plastic hinges form in the flanges. The flange anchorage lengths s_c and s_r are determined from static equilibrium at that state to

$$s_c=\frac{2}{\cos\partial}\sqrt{\frac{M_{pc}}{\sigma_{bb}\cdot t_w}} \tag{3a}$$

and

$$s_r=\frac{2}{\sin\partial}\sqrt{\frac{M_{pr}}{\sigma_{bb}\cdot t_w}} \tag{3b}$$

where ∂ is the angle of inclination of the diagonal LJ [Fig. 2(b)]; M_{pc} and M_{pr} are the plastic moments of beam and column flanges; and σ_{bb} is the tension field stress.

The stress of the tension field is equal to the yield stress allowing for the presence of shear stress due to the first mechanism, which yields

$$\sigma_{bb}=\sqrt{f_{yw}^2+\tau_{bb}^2(1{\cdot}5^2\sin^2 2\partial-3)}-1{\cdot}5\,\tau_{bb}\cdot\sin 2\partial \tag{4}$$

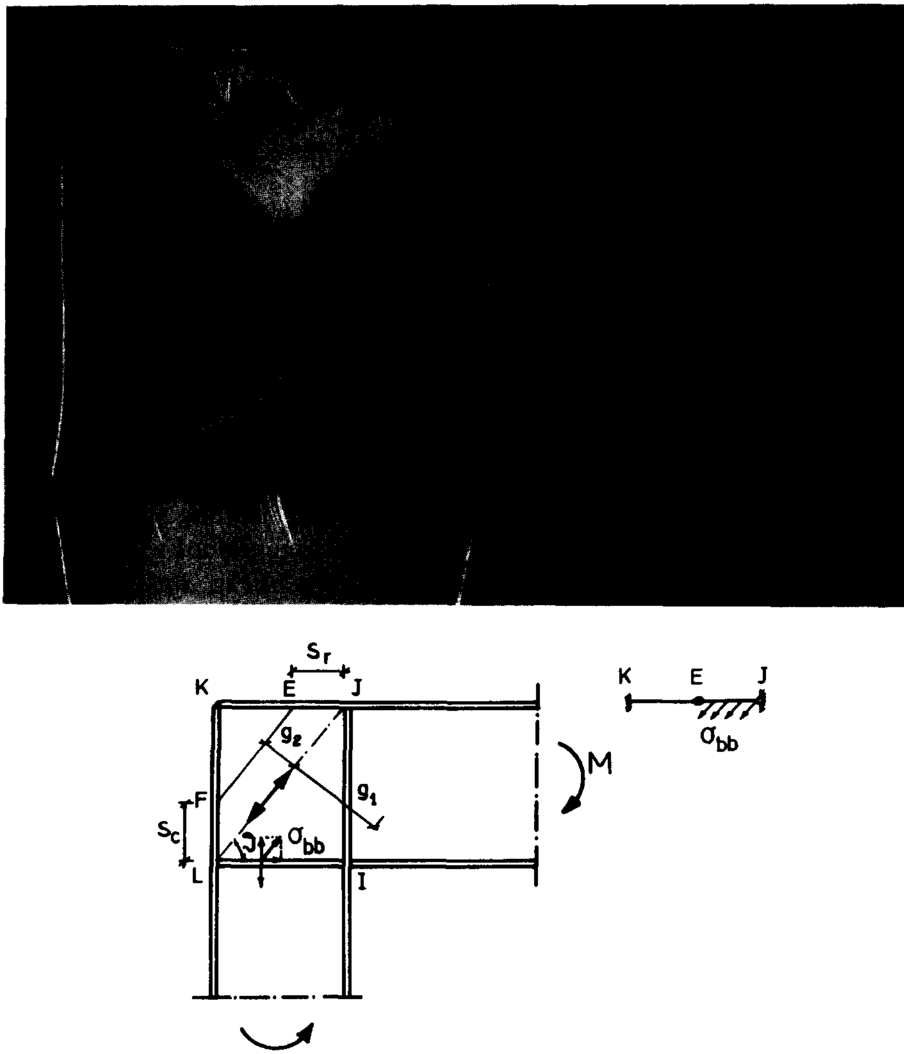

Fig. 2. Tension field for positive moments.

The width, g, of the tension field can be found from geometric relationships as

$$g = g_1 + g_2 = \min\{s_r \cdot \sin \vartheta,\ s_c \cdot \cos \vartheta\} + a \sin \vartheta \tag{5}$$

The joint moment M_{TF} due to tension field action is finally found from moment equilibrium around point I as

$$M_{TF}^{+} = \tfrac{1}{2} \cdot \sigma_{bb} \cdot t_w \cdot g^2 \tag{6}$$

After the completion of the tension field, any increase in joint-carrying capacity is due to the action of the frame surrounding the joint-panel. Applying the work equation for the frame yields the relevant joint moment as

$$M_{\mathrm{FR}} = M_{\mathrm{pr}} \cdot \frac{2a}{s_{\mathrm{r}}} + M_{\mathrm{pc}} \tag{7}$$

The ultimate joint moment, M_{u}, is finally found as the combination of the three mechanisms according to

$$M_{\mathrm{u}}^{+} = M_{\mathrm{bb}} + M_{\mathrm{TF}} + M_{\mathrm{FR}} \tag{8}$$

A comparison of the analytical results with the experimental corresponding ones of the 12 cyclic tests reported in ref. 5 showed for the $M_{\mathrm{u}}^{+\mathrm{exp}}/M_{\mathrm{u}}^{+\mathrm{th}}$ ratio a mean value of 1·05 and a standard deviation of 0·12.

Table 1 summarises the main geometrical and mechanical data of the

TABLE 1
Data of Specimen in mm, N/mm²

No.	*Specimen*	a	b	t_{w}	f_{yw}	t_{r}	t_{c}	f_{yr}	f_{yc}	$b_{\mathrm{r}}, b_{\mathrm{c}}$
1	AZ 05-10-2	200	200	1·03	230	5·05	5·05	304	304	150
2	AZ 10-10-1	200	200	1·02	230	9·70	9·70	278	278	150
3	CZ 10-10-H	240	300	1·03	226	9·70	9·70	275	275	150
4	CZ 10-10-Q	300	240	1·03	226	9·70	9·70	283	283	150
5	DZ 05-10-H	200	300	1·04	226	4·90	9·65	332	270	150
6	DZ 05-10-Q	300	200	1·02	230	9·65	4·90	270	332	150
7	B 03-20-1	300	300	2·0	310	3·0	3·0	232	232	150
8	B 03-20-02	300	300	2·0	319	5·1	3·0	324	232	150
9	B 03-20-3	300	300	2·0	319	5·0	3·0	324	232	150 90
10	F 05-20-1	150	299	2·0	319	3·0	5·0	232	324	149
11	C 03-20-1	240	300	2·0	319	3·0	3·0	232	232	150
12	C 05-20-1	240	300	2·0	319	5·2	5·2	324	324	149

TABLE 2
Comparison between Experimental and Theoretical Results

No.	*Positive moments* (kNm)						*Negative moments* (kNm)			
	M_{bb}	M_{TF}	M_{FR}	M_u^{th}	M_u^{exp}	M_u^{exp}/M_u^{th}	M_{TF}	M_u^{th}	M_u^{exp}	M_u^{exp}/M_u^{th}
1	1·9	4·1	1·3	7·3	7·8	1·07	3·9	5·8	6·9	1·19
2	1·9	6·4	2·9	11·2	12·9	1·15	7·1	9·0	12·1	1·34
3	2·1	10·6	3·6	16·0	17·5	1·10	10·5	12·2	16·2	1·33
4	2·1	10·4	3·0	15·5	15·4	1·00	10·5	12·2	14·4	1·18
5	2·0	5·7	2·2	9·9	12·1	1·22	6·9	8·9	10·1	1·13
6	2·0	5·6	2·2	9·8	12·1	1·23	6·9	8·9	9·9	1·11
7	14·7	10·9	1·2	26·8	25·6	0·96	4·6	19·3	20·8	1·08
8	14·7	10·9	1·2	27·0	24·5	0·91	6·8	21·5	22·4	1·04
9	14·7	10·9	1·2	26·9	25·6	0·95	5·8	20·5	20·5	1·00
10	11·0	3·8	0·9	15·7	18·9	1·20	3·6	14·6	17·4	1·19
11	15·2	7·2	1·0	23·4	22·2	0·95	3·7	18·9	20·2	1·07
12	15·2	9·4	2·1	26·7	24·0	0·90	7·2	22·4	24·0	1·07

experimental specimen; Table 2 the relevant theoretical and experimental results.

The yield moment, M_y, may be approximately determined as the corresponding ultimate moment, excluding the contribution of the frame action mechanism, since its mobilisation is accompanied by large joint rotations and a drop in stiffness. This gives

$$M_y^+ = M_{bb} + M_{TF}^+ \tag{9}$$

4 JOINT RESISTANCE FOR NEGATIVE MOMENTS

The joint-carrying capacity for negative moments ('opening' of the joint) may be determined by the same procedure as for positive moments. For that loading, it is suggested, however, to exclude the contribution of the frame action. The reason is that for negative moments a drop in carrying capacity after the attainment of the ultimate moment has been observed during the cyclic tests, due to an appearance of second order effects in the joint. These effects are caused by deviation forces in the flanges anchoring the tension field, which, for negative moments, are subjected to compression. These deviation (or second order) forces grow as the joint rotation increases. This is due to imperfections in the flanges caused by the plastic hinge's rotation in the compression flange from the previous loading cycle [Fig. 3(a)].

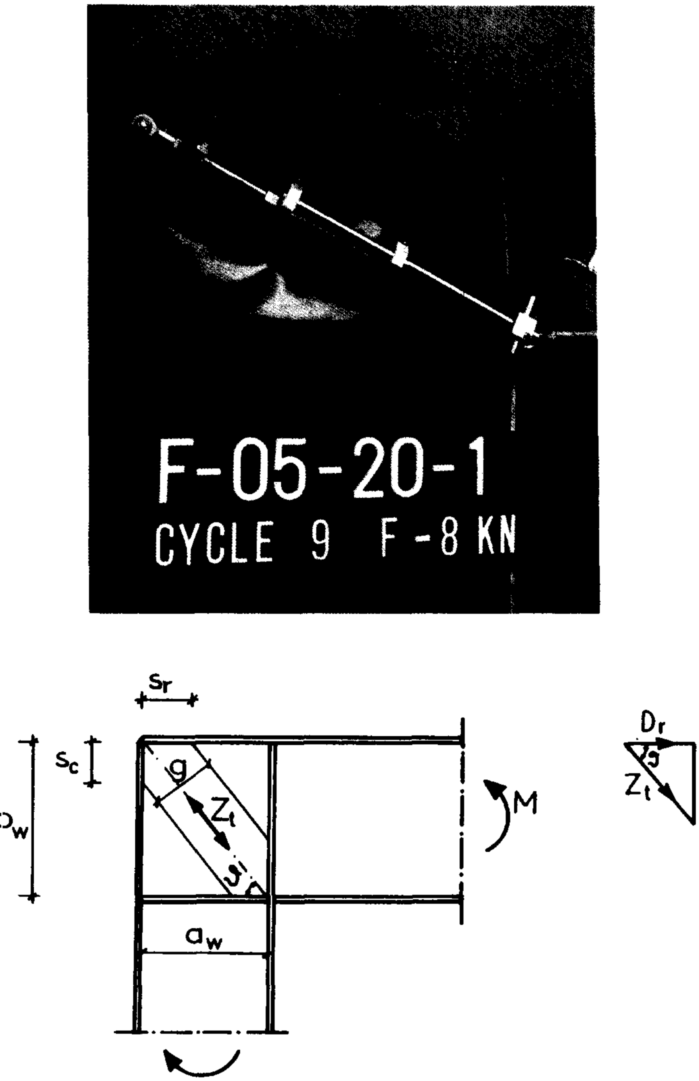

Fig. 3. Tension field for negative moments.

The second order effects are significant for joints with strong joint-panel and weak flanges. In the opposite case, a neglect of the frame action leads to an underestimation of the carrying capacity of the joint.

The shear buckling resistance for negative moments is the same as for positive moments. However, in this case the tension field action is lower, since the entire tension field force must be anchored by the flanges and the width of the tension field is accordingly smaller than for positive moments [Fig. 3(b)].

The tension field force, Z_t, is given as

$$Z_t^- = \sigma_{bb} \cdot t_w \cdot g = 2\sqrt{\sigma_{bb} \cdot t_w}\,(\sqrt{M_{pr}} + \sqrt{M_{pc}}) \tag{10}$$

where the tension field stress σ_{bb} is determined according to eqn (4).

The joint resistance due to tension field action is equal to

$$M_{TF}^- = Z_t^- \cdot \cos \partial \cdot b = 2\sqrt{\sigma_{bb} \cdot t_w}(\sqrt{M_{pr}} + \sqrt{M_{pc}}) \cdot \frac{ab}{d} \tag{11}$$

where d is the diagonal length, and the overall joint resistance for negative moments

$$M_u^- = M_{bb} + M_{TF}^- \tag{12}$$

A similar comparison between analytical and experimental results, as for positive moments, showed for the $M_u^{-\exp}/M_u^{-\text{th}}$ ratio a mean value of 1·13 and a standard deviation of 0·11. A detailed comparison is found in Table 2.

The yield moment may be approximately determined according to eqn (12), using, however, the flange yield moments in eqn (11) instead of their plastic moments.

5 JOINT DEFORMABILITY

The joint characteristic for monotonic loading may be approximated by a trilinear moment–rotation diagram, as shown in Fig. 4(a). The strain ε of

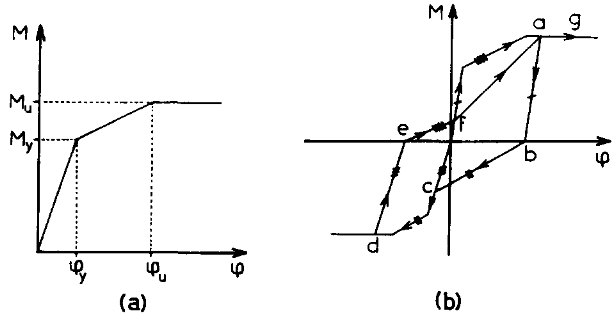

Fig. 4. Joint characteristics (a) for monotonic and (b) for cyclic loading.

the tensile joint-panel diagonal at a joint rotation φ is equal to

$$\varepsilon = \frac{a \cdot b}{d^2} \cdot \sin \varphi \tag{13}$$

As an approximation, the yield rotation φ_y may be defined as the rotation for which the strain is equal to the conventionally defined yield strain of $2^0/_{00}$, which gives

$$\varphi_y = 2^0/_{00} \cdot \left(\frac{a}{b} + \frac{b}{a}\right) \tag{14}$$

For an estimation of the ultimate rotation, φ_u, the following considerations may be taken into account. According to the ECCS Recommendations (1986), the yield moment is conventionally defined as the intersection between the initial elastic line with the tangent of the M–φ curve that has a slope equal to 1/10 of the slope of the initial elastic line. If this definition is applied to an approximate trilinear diagram, the post-yielding stiffness of the joint will be overestimated, since the resulting diagram will envelope the actual M–φ curve. Taking into account an experimentally observed factor of 3 for the slope, the expression for the ultimate rotation becomes

$$\varphi_u = \varphi_y + 3{\cdot}10\left(\frac{M_u}{M_y} - 1\right)\varphi_y \tag{15}$$

The hysteretic joint behaviour, as observed during the tests, may be approximately described as in Fig. 4(b). The trilinear joint characteristic, as discussed before for monotonic loading, is the skeleton line. This line is followed for the part of each loading that extends beyond the maximum deformation reached during a previous cycle (points a, d and g). Unloading occurs initially under the initial, elastic stiffness. The joint-panel flattens subsequently as the tension field along the one diagonal disappears and a new tension field along the opposite diagonal develops. This transition occurs approximately between the change of loading sign (points b and e) and the skeleton line (points c and f) at a reduced stiffness which is approximately set to the post-yielding stiffness. Actually, the change of stiffness does not occur at zero moments, as proposed here, but at moments corresponding to the shear-carrying capacity of the panel. These moments are, however, for the slender joint-panels examined here, very small and are decreased even more at each new cycle, due to panel imperfections, thus justifying the current proposal. The joint stiffness again increases when a new tension field along the opposite diagonal develops. The new stiffness is variable as the loading curve is directed towards the extreme point of the previous cycle (point a). Afterwards the skeleton line, as discussed before, is followed.

The experimental results showed that the proposed hysteretic behaviour is valid for joints with slender panels and a strong surrounding frame. The ductility of joints with slender panels and weak flanges is poor, since the capacity of the flanges to anchor the tension fields is very low. Additionally, for negative moments at higher rotations, second order effects further decrease the joint ductility. The application of such joints is therefore not recommended in high seismicity regions. A relevant cyclic characteristic is also not proposed here.

The distinction between strong and weak flanges may be undertaken with respect to the carrying capacity of the various mechanisms contributing to the joint resistance. The tests indicated that, as a first approximation, the moments due to shear buckling and tension field action, M_{bb}^{-} and M_{TF}^{-} respectively, may be used. If the former moment is larger than the latter, the flanges may be considered to be weak, or strong in the opposite case.

6 ANALYSIS OF FRAMES WITH FLEXIBLE JOINT-PANELS

In a conventional analysis of sway frames, it is usually assumed that the joints are rigid and of negligible dimensions, so that frames are represented by member centre lines. In the case of slender joint-panels, as examined here, the joint deformability should be taken into account in frame analysis, as it has an influence on the strength and stability of the frame, this will be done subsequently using a model for the joint as proposed by Ermopoulos and Vayas.[8] This model can describe, through appropriate springs, the flexibility of both the connections and the joint-panel. In the present analysis, only the joint-panel flexibility will be considered. For the calibration of the model against experimental results, a frame configuration representing the testing arrangement, as described in ref. 5, will be considered (Fig. 5). The analysis takes into account non-linearities arising from both geometrical and material non-linear effects. It is, as in the tests, strain-controlled by application of deformation cycles at the end of the beam. The cyclic pattern corresponds to the experimental one, as proposed by the ECCS 'Recommended Testing Procedure' (1986), with the difference that only one, instead of three, cycle has been applied for a specific ductility level.

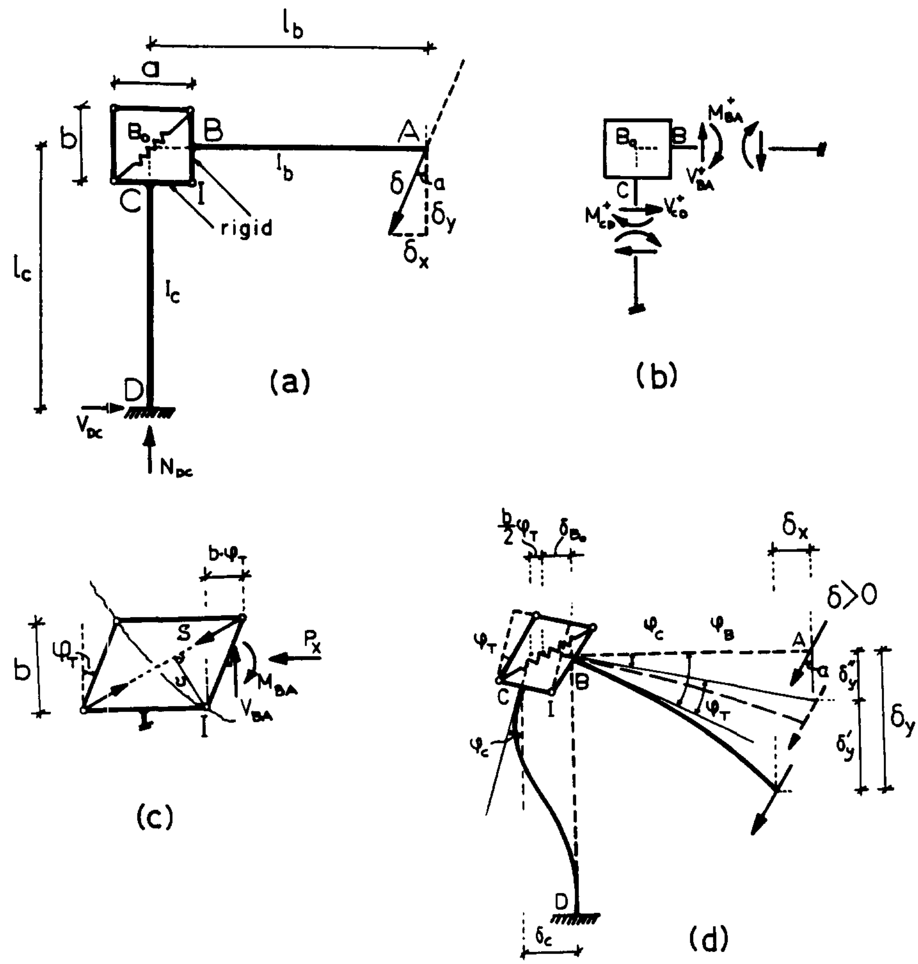

Fig. 5. Frame under consideration and sign convention according to slope-deflection method.

The force–displacement relationship of the frame at the free end A may be written as

$$\delta_x = \delta'_x - \delta''_x = \frac{P_x \cdot l_c^3}{3EI_c} - \frac{P_y \cdot l_b \cdot l_c^2}{2EI_c} \tag{16}$$

and

$$\delta_y = \delta'_y + \delta''_y = l_b \cdot \tan \varphi_c + \frac{P_y \cdot l_b^3}{3EI_b} \tag{17}$$

where δ'_x = horizontal column deflection due to the force P_x; δ''_x = horizontal column deflection due to a moment $P_y l_b$ at its top; δ'_y = vertical beam deflection due to column rotation φ_{B_0} when the joint is considered as rigid; and δ''_y = vertical beam deflection due to the force P_y; I_b, I_c, l_b, l_c = moments of inertia and axis lengths of beam and column, respectively.

In the above relations, the beam and column lengths have been approximately considered at centre lines.

The rotation of the column top, φ_c, due to application of a force P_x and a moment $P_y \cdot l_b$ is equal to

$$\varphi_c = \frac{P_y \cdot l_b \cdot l_c}{EI_c} - \frac{P_x l_c^2}{2EI_c} \tag{18}$$

which substituted into eqn (17) gives the final force–displacement relationship for the point A.

Taking into account the joint rotation, φ_T, due to the joint-panel deformations, the sway of the frame is given by

$$\delta_c = \delta_x + \frac{b}{2} \cdot \varphi_B = \delta \cdot \sin a + \frac{b}{2}(\varphi_c + \varphi_T) \tag{19}$$

thus establishing a relationship between the applied displacements, δ, and the frame sway, δ_c, having φ_c and φ_T as unknowns. These unknown rotations may be determined by application of two further equations. These are the moment equations around the points of member intersection B_0, and the internal corner of the joint I.

The corresponding equations are

$$M_{CD} - V_{CD}\frac{b}{2} + M_{BA} - V_{BA}\frac{a}{2} = 0 \tag{20}$$

and

$$S_n \cdot u_n + P_x \frac{b}{2} + V_{BA}\frac{b}{2}\varphi_T - M_{BA} = 0 \tag{21}$$

The beam and column moments, M_{BA} and M_{CD}, and shear forces, V_{BA} and V_{CD}, are expressed in terms of the member end-displacements and rotations using the generalised slope–deflection equations shown in Appendix 1. In these equations the clear member lengths are used.

The spring characteristic is written in linearised, incremental form as

$$S_n = S_o + r_n(d_n - d_o) \tag{22}$$

where r_n is the actual spring stiffness determined in accordance with the hysteretic model of the joint-panel described before.

The actual spring length, d_n, and lever arm of the spring, u_n, with respect to point I, are functions of the joint rotation due to its panel flexibility. They are determined from

$$d_n = \frac{ab}{d}\varphi_T + d_o \tag{23}$$

and

$$u_n = \frac{ab \cdot d(1 - \varphi_T^2/2)}{d^2 + ab\varphi_T} \tag{24}$$

Substituting eqns (22), (23) and (24), as well as the slope–deflection equations (appropriately arranged for this particular case) into eqns (20) and (21), finally results in a system of two equations for the unknown rotations φ_c and φ_T. This system is solved iteratively at each loading step, thus allowing the determination of the new force and deformation values (n) from the old ones (o).

7 NUMERICAL RESULTS

The numerical results refer to joints that have been tested experimentally, in order to allow for a comparison between analytical and experimental results. Due to the overall dimensions of the testing arrangement, as described in ref. 5, the entire frame flexibility may be assigned to the joint-panel deformations. The frame response is described accordingly, as in the tests, by moment–rotation curves of the joint, rather than by force–displacement curves of the frame.

For each test, two analyses will be performed. In the first, the ultimate and yield moments and rotations used for the establishment of the trilinear joint characteristic will be evaluated from the test results. In the second, analysis of the relevant values will be determined analytically using the proposed formulae. Analysis 1 may serve for an evaluation of the hysteretic joint model. Analysis 2 describes the frame behaviour in cases where corresponding test results are not available.

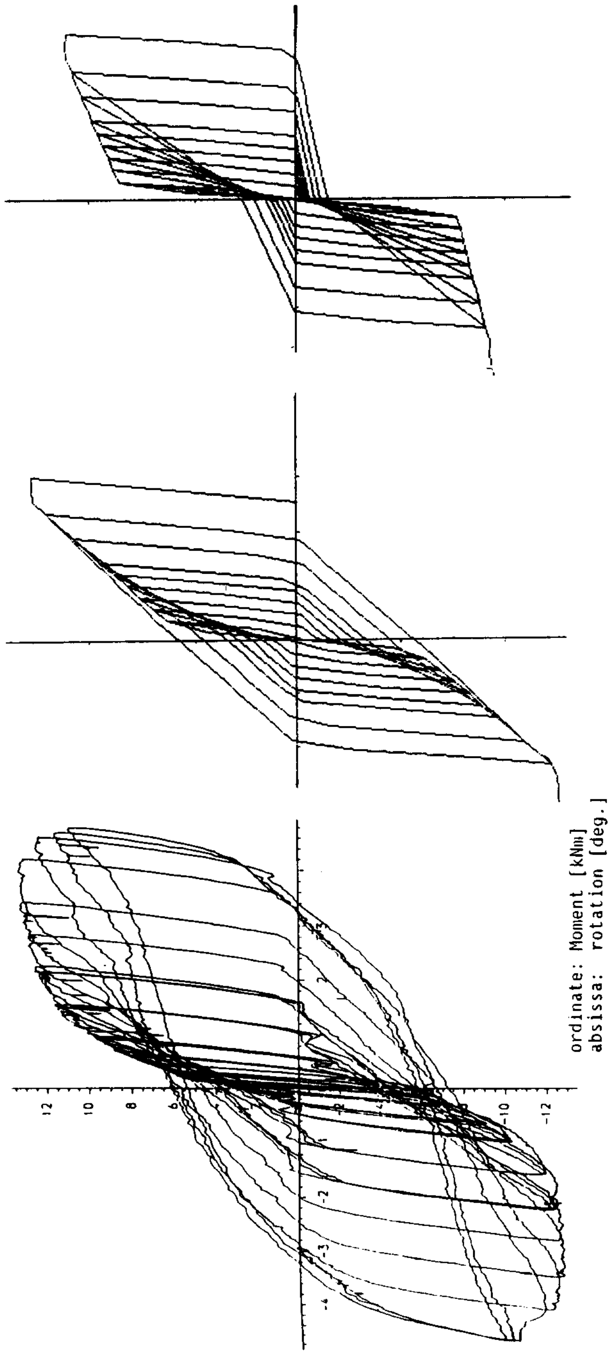

Fig. 6. Hysteresis loops for joint AZ10101: (a) experimental; (b) analysis 1; (c) analysis 2.

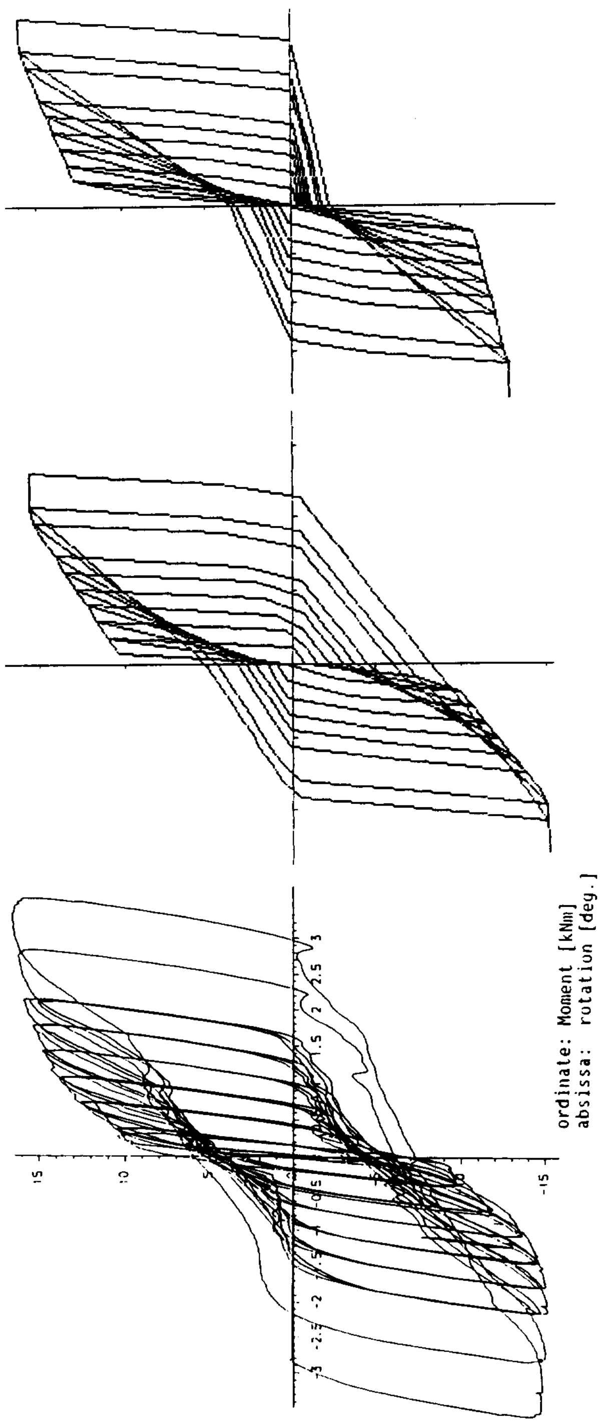

Fig. 7. Hysteresis loops for joint CZ1010Q: (a) experimental; (b) analysis 1; (c) analysis 2.

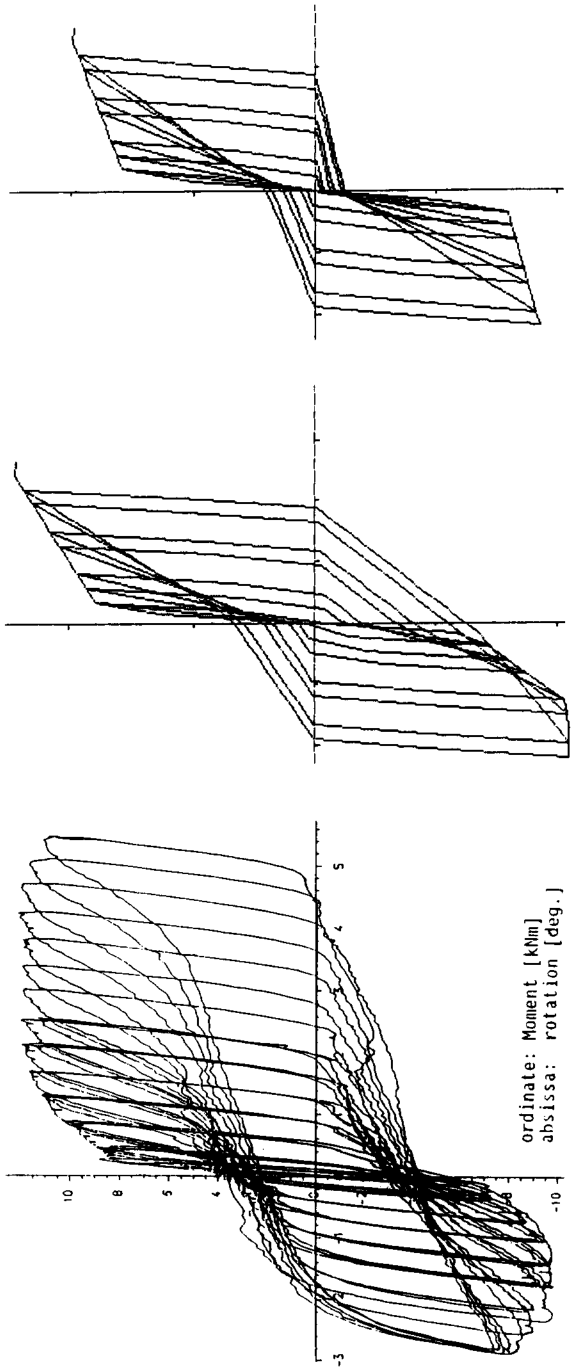

Fig. 8. Hysteresis loops for joint DZ0510Q: (a) experimental; (b) analysis 1; (c) analysis 2.

A comparison between experimental and analytical results for three specimens is shown in Figs 6–8. A detailed numerical example for the evaluation of the moments and rotations of one joint is given in Appendix 2.

A certain discrepancy occurs in the region where a tension field flattens and before a new tension field develops in the opposite direction, the actual stiffness seems to be lower than the predicted one. However, regarding the complexity of the problem, the analytical predictions may be considered as satisfactory.

8 SUMMARY AND CONCLUSIONS

The purpose of this paper is to access the behaviour of thin-walled, slender joint-panels in knee joints of steel frames and to evaluate how it effects the overall moment-resisting frame.

The joint resistance is supplied by three mechanisms, namely the shear buckling-carrying capacity of the joint-panel, the tension field action and the frame action of the elements surrounding the panel. Based on experimental evidence, relevant design formulae have been proposed. While the first mechanism is provided by the joint-panel and the third mechanism by the frame alone, the extent of the tension field mechanism is dependent on the relative proportions of the joint-panel to the surrounding flanges.

Monotonic and hysteretic rules for the joint have been proposed that allow for the description of joint characteristics, if they are to be included in a frame analysis. Using an appropriate frame analysis model, a simple frame was analysed considering its nonlinear behaviour due to geometric effects and the influence of the joint behaviour due to joint-panel deformations. The application of the method has been shown for some tested joints.

ACKNOWLEDGEMENT

Partial support in the preparation of this paper was provided by the Greek General Secretariat for Research and Technology and the Forschungszentrum Julich GmbH under grants available for a bilateral German–Greek scientific co-operation.

REFERENCES

1. Chen, W. F. (ed.), *Joint Flexibility in Steel Frames.* Elsevier Applied Science, London, 1987.
2. Bjorhovde, R., Brozzetti, J. & Colson, A. (eds), *Connections in Steel Structures.* Elsevier Applied Science, London, 1988.
3. Kato, B., Chen, W. F. & Nakao, M., Effects of joint-panel shear deformation on frames. *J. Constr. Steel Res.*, **10** (1988) 269–320.
4. Scheer, J., Pasternak, H. & Schween, T., Structural behaviour of stiffened knee joints with thin webs. *J. Struct. Engng*, **117**(9) (1991) 2600–2619.
5. Vayas, I., Pasternak, H. & Schween, T., Cyclic behavior of beam-to-column steel joints with slender web panels. *J. Struct. Engng* (to be published).
6. Scheer, J., Pasternak, H. & Schween, T., *Ermittlung der Traglast von geschweissten Rahmenecken mit Hilfe von Zugfeldmodellen.* Institut fur Stahlbau, Technische Universitat Braunschweig, Report 6202/2, 1992.
7. Eurocode 3. *Design of Steel Structures*, ENV 1993-1-1, 1992.
8. Ermopoulos, J. & Vayas, I., Nachweis von Rahmentragwerken mit verformbaren Knoten. *Stahlbau*, **60** (1991) 326–332.

APPENDIX 1: SLOPE–DEFLECTION METHOD EQUATIONS

The moments and shear forces at the member ends taking into account the axial load are given by the following equations (Fig. A1)

$$M_{ij} = \frac{2EI}{l}\left[a_n \varphi_i + a_f \varphi_j + (a_n + a_f)\frac{\delta_i - \delta_j}{l}\right] \qquad \text{(A1)}$$

$$M_{ji} = \frac{2EI}{l}\left[a_f \varphi_i + a_n \varphi_j + (a_n + a_f)\frac{\delta_i - \delta_j}{l}\right] \qquad \text{(A2)}$$

$$V_{ij} = V_{ji} = \frac{M_{ij} + M_{ji}}{l} - N\frac{\delta_i - \delta_j}{l} \qquad \text{(A3)}$$

$$a_n = \frac{\varphi_n}{2(\varphi_n^2 - \varphi_f^2)}, \qquad a_f = \frac{\varphi_f}{2(\varphi_n^2 - \varphi_f^2)} \qquad \text{(A4)}$$

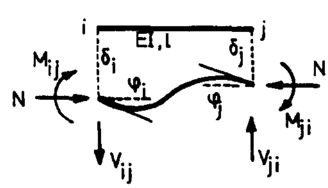

Fig. A1. Sign convention for slope-deflection method.

$$\beta^2 = \frac{Nl^2}{EI} \tag{A5}$$

If N is compressive, then

$$\varphi_n = \frac{1-\beta/\tan\beta}{\beta^2}, \qquad \varphi_f = \frac{\beta/\sin\beta - 1}{\beta^2} \tag{A6}$$

If N is tensile, then

$$\varphi_n = \frac{\beta/\tanh\beta - 1}{\beta^2}, \ \varphi_f = \frac{1-\beta/\sinh\beta}{\beta^2} \tag{A7}$$

APPENDIX 2: EXAMPLE

The calculation procedure for the determination of the joint resistance and flexibility is shown using the data from one of the tests (CZ 10.10.Q, ref. 5).

Material, geometry

$$a = 300\,\text{mm} \tag{A8}$$
$$b = 240\,\text{mm} \tag{A9}$$
$$t_w = 1{\cdot}03\,\text{mm} \tag{A10}$$
$$f_{yw} = 22{\cdot}6\,\text{kN/cm}^2 \tag{A11}$$
$$t_f = 9{\cdot}7\,\text{mm (flange thickness)} \tag{A12}$$
$$b_f = 150\,\text{mm (flange width)} \tag{A13}$$
$$f_{yf} = 28{\cdot}3\,\text{kN/cm}^2\ \text{(flange yield strength)} \tag{A14}$$

$$\partial = \arctan\frac{240}{300} = 38{\cdot}6^\circ \tag{A15}$$

$$\frac{a}{b} = \frac{300}{240} = 1{\cdot}25 > 1 \tag{A16}$$

$$K_\tau = 5{\cdot}34 + \frac{4}{(a/b)^2} = 5{\cdot}34 + \frac{4}{1{\cdot}25^2} = 7{\cdot}9 \tag{A17}$$

$$\tau_{cr} = 7{\cdot}9 \cdot 18980\left(\frac{1{\cdot}03}{240}\right)^2 = 2{\cdot}76\,\text{kN/cm}^2 \tag{A18}$$

$$\bar{\lambda} = \sqrt{\frac{22{\cdot}6/\sqrt{3}}{2{\cdot}76}} = 2{\cdot}17 > 1{\cdot}25 \tag{A19}$$

$$\tau_{bb} = \tau_{cr} = 2{\cdot}76\ \text{kN/cm}^2 \tag{A20}$$

$$M_{bb} = 30 \cdot 24 \cdot 0{\cdot}103 \cdot 2{\cdot}76 = 205\ \text{kN cm} \tag{A21}$$

$$\sigma_{bb} = \sqrt{22{\cdot}6^2 + 2{\cdot}76^2[1{\cdot}5^2 \cdot \sin^2(2 \cdot 38{\cdot}6) - 3]} - 1{\cdot}5 \cdot 2{\cdot}76 \cdot \sin(2 \cdot 38{\cdot}6) = 18{\cdot}4\ \text{kN/cm}^2 \tag{A22}$$

$$M_{pc} = M_{pr} = \frac{15 \cdot 0{\cdot}97^2}{4} \cdot 28{\cdot}3 = 99\ \text{kN cm} \tag{A23}$$

$$s_c \cdot \cos \partial = s_r \cdot \sin \partial = 2\sqrt{\frac{99}{18{\cdot}4 \cdot 0{\cdot}103}} = 14{\cdot}5\ \text{cm} \tag{A24}$$

$$g = 14{\cdot}3 + 30 \sin 38{\cdot}6^\circ = 33{\cdot}2\ \text{cm} \tag{A25}$$

$$M_{TF}^{+} = \tfrac{1}{2} \cdot 18{\cdot}4 \cdot 0{\cdot}103 \cdot 33{\cdot}2^2 = 1044\ \text{kN cm} \tag{A26}$$

$$s_r = 14{\cdot}5/\sin 38{\cdot}6^\circ = 23{\cdot}2\ \text{cm} \tag{A27}$$

$$M_{FR} = 99 \cdot \frac{2{\cdot}24}{23{\cdot}2} + 99 = 304\ \text{kN cm} \tag{A28}$$

$$M_u^{+} = 205 + 1044 + 304 = 1553\ \text{kN cm} = 15{\cdot}53\ \text{kN m} \tag{A29}$$

(experimental value $M_u^{+} = 15{\cdot}4$ kN m)

$$M_y^{+} = 205 + 1044 + 1249\ \text{kN cm} = 12{\cdot}49\ \text{kN m} \tag{A30}$$

(experimental value $M_y^{+} = 10$ kN m)

$$M_{TF}^{-} = 2\sqrt{18{\cdot}4 \cdot 0{\cdot}103}\,(\sqrt{97} + \sqrt{97}) \cdot \frac{30 \cdot 24}{\sqrt{30^2 + 24^2}} = 1016\ \text{kN cm} \tag{A31}$$

$$M_u^{-} = 205 + 1016 = 1221\ \text{kN cm} = 12{\cdot}21\ \text{kN m} \tag{A32}$$

(experimental value $M_u^{-} = 14{\cdot}4$ kN cm)

$$M_y^{-} = 205 + \frac{1016}{\sqrt{1.5}} = 1034\ \text{kN/cm} = 10{\cdot}34\ \text{kN m} \tag{A33}$$

(experimental value $M_y^- = 9{\cdot}0$ kN m)

$$\varphi_y = 2‰\left(\frac{300}{240}+\frac{240}{300}\right)=0{\cdot}0041 \text{ rad} = 0{\cdot}23° \tag{A34}$$

$$\varphi_u^+ = 0{\cdot}23+3\cdot 10\left(\frac{1538}{1238}-1\right)0{\cdot}23 = 1{\cdot}94°$$

$$\varphi_u^- = 0{\cdot}23+3\cdot 10\left(\frac{1221}{1034}-1\right)0{\cdot}23 = 1{\cdot}48° \tag{A35}$$